Combustion and Flame 197 (2018) 319–327

Contents lists available at ScienceDirect

Combustion and Flame

journal homepage: www.elsevier.com/locate/combustflame

Effect of aluminum micro- and nanoparticles on ignition and combustion properties of energetic composites for interfacial bonding of metallic substrates

Kyung Ju Kim[a], Myung Hoon Cho[a], Soo Hyung Kim[a,b,*]

[a] Department of Nano Fusion Technology, College of Nanoscience and Nanotechnology, Pusan National University, 30 Jangjeon-dong, Geumjung-gu, Busan 609-735, Republic of Korea

[b] Department of Nanoenergy Engineering, College of Nanoscience and Nanotechnology, Pusan National University, 30 Jangjeon-dong, Geumjung-gu, Busan 609-735, Republic of Korea

ARTICLE INFO

Article history:
Received 17 December 2017
Revised 29 June 2018
Accepted 22 August 2018

Keywords:
Energetic materials
Solder materials
Multilayer pellets
Exothermic reactions
Interfacial bonding

ABSTRACT

In this study, the effect of micro- and nanoscale energetic materials in the formulation of aluminum microparticles (Al MPs)/aluminum nanoparticles (Al NPs)/iron oxide nanoparticles (Fe_2O_3 NPs) as a heat energy source for melting solder microparticles (SAC 305 MPs) on the interfacial bonding properties of Cu metallic substrates, is investigated. The optimized mixing ratio is Al MP:Al NP:Fe_2O_3 NP = 30:30:40 wt%, which generates a maximum total exothermic energy of ~2.0 kJ g^{-1}. The presence of Al NPs is essential to make stable ignition and initiation of Al MPs, which enable to attain relatively long combustion duration. The use of highly reactive Al NPs/Fe_2O_3 NPs can improve the aluminothermic reaction, while the addition of Al MPs to the Al NPs/ Fe_2O_3 NPs is also required to maintain their high thermal energy for a longer duration. An energetic material (EM) layer composed of Al MP/Al NP/Fe_2O_3 NP composites is employed as a heat source between solder material (SM) layers composed of SAC305 MPs. The SM/EM/SM multilayer pellets are assembled and ignited between interfacial Cu substrates for bonding. Thus, interfacial bonding between the Cu substrates is successfully achieved, and the resulting maximum mechanical strength for the bonded Cu substrates using the SM/EM/SM multilayer pellets increases by ~40% compared to that when using a pure SM layer pellet. Hence, EM layers can act as both an effective heat energy generation source and a mechanical reinforcing medium, while the interfacial bonding process using SM/EM/SM multilayer pellets demonstrated herein provides an easy and versatile means of welding and jointing for industrial applications.

1. Introduction

Several interfacial bonding processes, such as anodic bonding, direct bonding, solder bonding, and adhesive bonding, have been developed [1–7]. For these processes, the interfacial bonding properties (including the bonding strength and airtightness) are highly dependent on the bonding conditions, including the temperature, pressure, and type of substrate [8–15]. In particular, soldering with molten solder at high temperatures inherently creates compounds between the solder and substrate, which can affect the interfacial bonding properties [16–18]. High-temperature conditions can release residual stresses in multi-layered bonding substrates, while they can simultaneously result in a weakening of the interfacial bonding strength [19,20]. When low-pressure conditions are applied, the actual contact area between the interfacial bonding parts can be reduced, and thus, this can result in a significant decrease in the interfacial bonding strength. Therefore, the interfacial bonding process generally requires a closed system, in which temperature- and pressure-controlled conditions are applied to both the solder and interfacial substrates [21,22].

Generally, a heat source, such as a furnace, welding torch, or microwave plasma burner is employed to preheat and coalesce the solder and substrate. For example, several bonding processes have been developed, including eutectic bonding, activated bonding, cast bonding and solid-state joining, which rely on the use of a furnace to supply heat energy. However, these are subject to a range of restrictions on the material selection and bonding structures. Simultaneously, to suppress the formation of cracks, defects, and residual stress for interfacial bonding, the precise control of the operating conditions, such as the preheating temperature, dwell time, and cooling rate, is also required [23]. However, relatively high

* Corresponding author at: Department of Nano Fusion Technology, College of Nanoscience and Nanotechnology, Pusan National University, 30 Jangjeon-dong, Geumjung-gu, Busan 609-735, Republic of Korea.
E-mail address: sookim@pusan.ac.kr (S.H. Kim).

https://doi.org/10.1016/j.combustflame.2018.08.016
0010-2180/

temperatures and pressures, applied over an extended duration, are usually adopted for interfacial bonding processes, so that the structural changes in the substrates to be bonded occur due to thermal deformation, surface oxidation, and the formation of intermetallic compounds between the solder and substrate. This can eventually result in reducing the mechanical strength while adversely affecting the physical properties of the bonded substrates [24–26].

Energetic materials (EMs) are composites consisting of fuel and an oxidizer. They store chemical energy, which can be rapidly turned into thermal energy via a homogeneous exothermic reaction when ignited by an external energy input [27–39]. The heat energy generated by the ignition of highly reactive EMs can be used to bond interfacial substrates by melting the solder inserted between those substrates. The use of EMs as a heat source for interfacial bonding offers several advantages including, (i) there is no need to heat either the solder or the interfacial substrates, (ii) additional, possibly complex, heating equipment is not necessary, and (iii) the simple and versatile interfacial bonding process can be implemented for a range of interfacial structures.

In the present study, we systematically investigated the effects of using EMs as a heat energy source on the interfacial bonding properties of metallic substrates. Solder material (SM) and EM were pelletized with multiple layers, and were then inserted between the metallic substrates to enable interfacial bonding. Specifically, micro- and nanoscale aluminum (Al) was used as the fuel, while iron oxide (Fe_2O_3) was used as a weak oxidizer. SAC 305 was used as a SM. Various SM/EM/SM multilayer pellets were fabricated and then tested to determine their efficacy at bonding the interfacial metallic substrates. The ignition, combustion, and physical properties of the SM/EM/SM multilayer pellets and the mechanical properties of the bonded Cu metallic substrates were systematically examined using several different techniques, including a high-speed camera, pressure-cell tester (PCT), differential scanning calorimetry (DSC), scanning electron microscopy (SEM) and universal tensile-strength testing.

2. Experimental

In the present study, a mixture of Al nanoparticles (Al NPs; Nano Technology Co., Ltd., Korea) with an average diameter of around 80 nm, and Al microparticles (Al MPs; Player Metal Co., Ltd., Korea) with an average diameter of around 8 μm, was used as the fuel source. As the oxidizer, we used Fe_2O_3 NPs (Sigma-Aldrich, Korea) with an average diameter of around 90 nm. SAC 305 powder (Sn: 96.5 wt%, Ag: 3 wt%, Cu: 0.5 wt%; Senju Metal Industry Co., Ltd., Japan) with an average diameter of around 70 μm was used as the SM.

Figure 1 is a schematic diagram of the fabrication of EMs composed of Al NPs, Al MPs, and Fe_2O_3 NPs. The SM/EM/SM multilayer pellets were formed by a subsequent die-compaction process. The fabricated SM/EM/SM multilayer pellets were inserted between the Cu substrates, and then the interfacial bonding process was implemented by igniting the multilayer pellets using a tungsten hot-wire with an applied voltage of around 4 V and a current of around 2 A.

Briefly, EM powders composed of Al NPs/Al MPs/Fe_2O_3 NPs were dispersed in an ethanol solution, and were subsequently mixed by ultrasonication (ultrasonic power ≈ 170 W, ultrasonic frequency ≈ 40 kHz) for 30 min with a mixing ratio of Al NP:Al MP:Fe_2O_3 NP = 30:30:40 wt%, which was empirically determined as the optimum combustion condition for exothermic reactions, as shown in Fig. S1 in Supporting information. The EM powders were finally dried in a convection oven at 80 °C for 30 min. EM (i.e., Al NP/Al MP/Fe_2O_3 NP composites) and SM (i.e., SAC305 MP, Sn: 96.5%, Ag: 3%, Cu: 0.5%) powders were sequentially poured into a mold in the die-compaction process, and were then pelletized into disks approximately 7 mm in diameter and around 1 mm in height under a pressure of 300 MPa.

Differential scanning calorimetry (DSC; Setaram, LABSYS evo, France) measurements of the EM powders were performed with a temperature increase rate of 10 °C min^{-1} at 30–1000 °C under an air atmosphere. The physical structure of the fabricated SM/EM/SM multilayer pellets was observed using scanning electron microscopy (SEM) (Carl Zeiss, Supra 40VP, Germany) operating at around 20 kV. The elemental mappings of interfacially bonded Cu substrates and EM powders were observed using a field emission scanning electron microscope equipped with an energy dispersive X-ray analyzer (EDS, INCA, Oxford Instruments, Abingdon, UK). The X-ray phase analyses of EM powders were performed using X-ray diffractometry (XRD, Empyrean series2, PANalytical, Almero, Netherlands) with Cu Kα radiation in the range of 20–90°. A high-speed camera (Photron, FASTCAM SA3 120 K, Japan) was employed to observe the ignition and combustion reaction of the EM powders and pellets fabricated in the present study. The high-speed camera had a maximum frame rate of 1,200,000 fps, a minimum frame rate of 60 fps, a 17.4 mm × 17.4 mm CMOS image sensor, a pixel size of 17 μm × 17 μm, and a AC operating voltage 100–240 V, drawing a current of 60 A. The PCT was used to analyze the pressure trace and pressurization rate by igniting the composite powders in a sealed pressure cell (around 13 ml). Briefly, EM powder (around 16 mg) was placed in the sealed pressure cell, and then ignited by using a tungsten hot-wire igniter, which was operated at around 4 V, drawing a current of 2 A. The explosion pressure generated by the hot-wire ignition was measured by a piezoelectric pressure sensor (113A03, PCB Piezotronics) attached to the pressure cell. Simultaneously, the detected pressure signal was amplified and transformed into a voltage signal through a combination of an in-line charge amplifier (422E11, PCB Piezotronics) and signal conditioner (480C02, PCB Piezotronics). Finally, the signal was captured and recorded using a digital oscilloscope (TDS 2012B, Tektronix). We calculated the pressurization rate by measuring the maximum pressure with the rise time when the composite powder was ignited. After performing the interfacial bonding process, the mechanical bonding strength of the Cu substrates was measured using a universal tensile strength tester (LRXPlus 5 kN, Lloyd Instruments Ltd., UK) with a strain rate of around 10 mm min^{-1}.

3. Results and discussion

Figure 2 shows the SEM images and energy dispersive X-ray spectroscopy (EDS) elemental mappings for the Al NP/Al MP/Fe_2O_3 NP composite powder used in the present study. The Al NPs and Al MPs, used as a fuel, were both spherical with average diameters of around 100 nm (Fig. 2a) and 8 μm (Fig. 2b), respectively. The Fe_2O_3 NPs, used as an oxidizer, were also spherical with an average diameter of around 90 nm (Fig. 2c). After mixing the Al NPs/Al MPs/Fe_2O_3 NPs, the resulting EM composite powders were observed using SEM and EDS, as shown in Fig. 2d–f. It was found that the Al NPs/Fe_2O_3 NPs were homogeneously distributed and attached to the surfaces of the Al MPs.

We systematically examined the effects of Al NPs and Al MPs on the ignition and combustion properties of EMs. Figure 3 shows schematics and still images of the ignition and combustion reactions of the EMs addressed in the present study. First, Al MP/Fe_2O_3 NP-based EMs without any Al NPs failed to ignite when using a tungsten hot-wire, even when heated to around 800 °C with an applied voltage of around 12 V [40,41]. This suggests that a high thermal energy input is required to directly ignite Al MPs, which have a relatively low reactivity due to their large primary size. However, when Al NPs were present in EMs (i.e., the Al NP/Fe_2O_3 NP and Al NP/Al MP/Fe_2O_3 NP composites), the ignition and subsequent combustion occurred stably using the same tungsten hot-wire heated

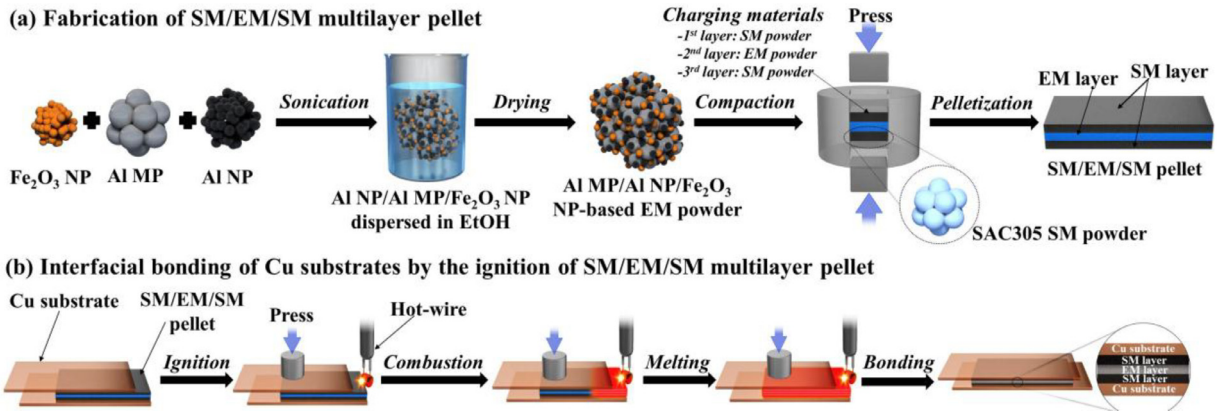

Fig. 1. (a) Fabrication of EMs composed of Al NPs, Al MPs, and Fe_2O_3 NPs, and the fabrication of SM/EM/SM multilayer pellets by a die-compaction process. (b) Interfacial bonding process using a SM/EM/SM multilayer pellet installed between metallic substrates.

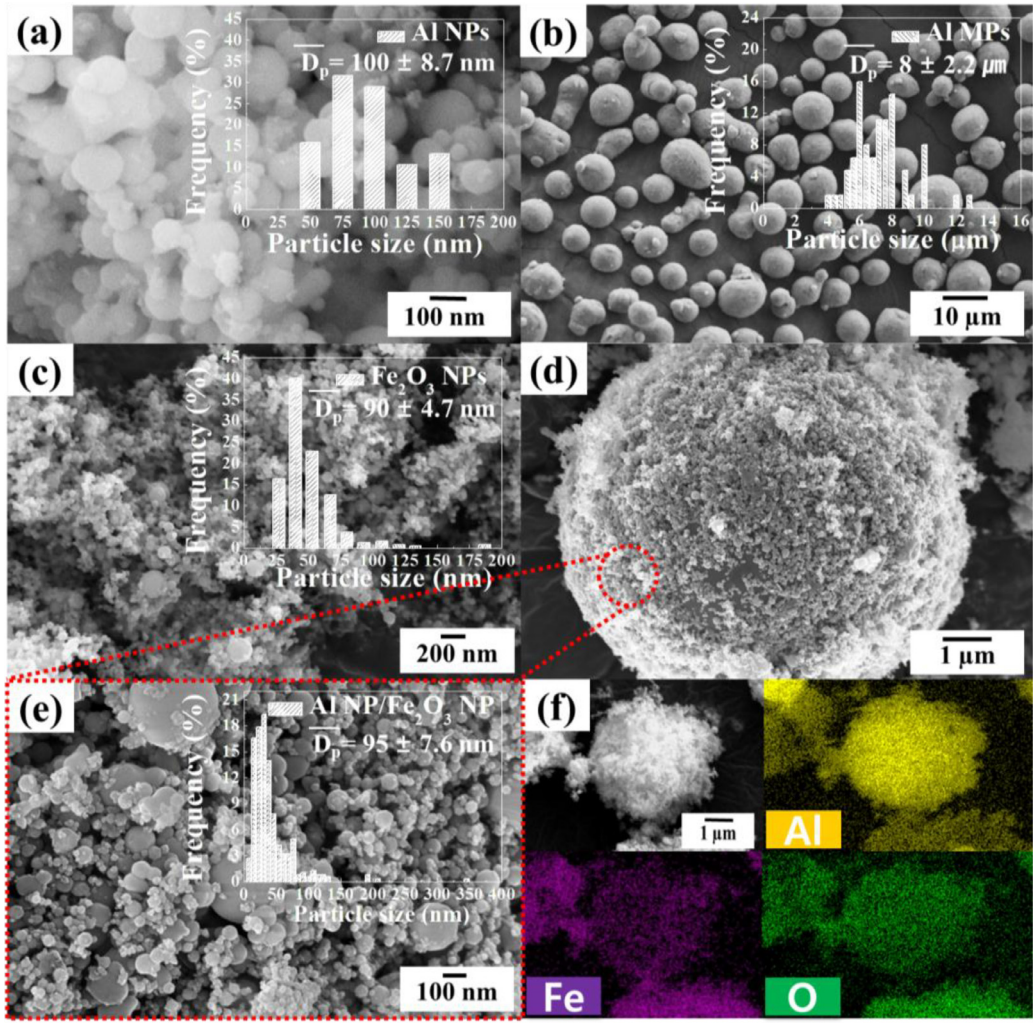

Fig. 2. SEM images of (a) Al NPs, (b) Al MPs, (c) Fe_2O_3 NPs. (d) LR-SEM image, (e) HR-SEM image, and (f) elemental mapping of Al NP/Al MP/Fe_2O_3 NP composites.

to around 560 °C with the application of around 4 V. The resulting burn rate and total burning time of Al NP/Fe_2O_3 NP were around 0.420 m s^{-1} and 120 ms, while those of Al NP/Al MP/Fe_2O_3 NP were around 0.084 m s^{-1} and 500 ms, respectively. (The burn rate was defined as the total length of the aligned EM pellet sample divided by the total time taken for the flame to propagate from one end of the pellet to the other.) This suggests that the presence of Al NPs resulted in the combustion reactivity of the EMs being enhanced, but the addition of Al MPs to the Al NP/Fe_2O_3 NP-based EMs made their combustion reactivity much slower. This is presumably because the exothermic energy generated by the burning Al NPs was consumed by initiating the Al MPs. Once the Al NP/Al MP/Fe_2O_3 NP composite pellets had been ignited, the combustion reaction was very slow and the flame propagation reached

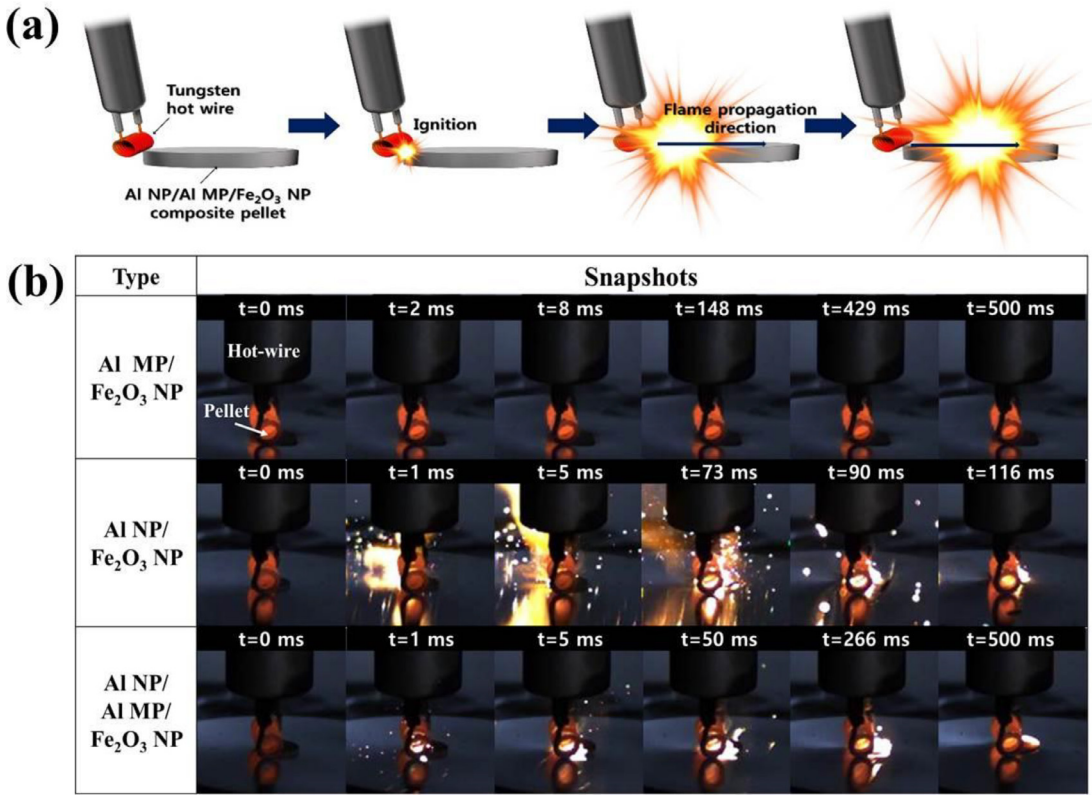

Fig. 3. (a) Schematics and (b) still images of tungsten hot-wire induced ignition and subsequent combustion of (i) Al MP (60 wt%)/Fe_2O_3 NP (40 wt%), (ii) Al NP (60 wt%)/Fe_2O_3 NP (40 wt%), and (iii) Al NP (30 wt%)/Al MP (30 wt%)/Fe_2O_3 NP (40 wt%) composite pellets.

the end of the pellets without stopping. If the functional EM pellets are to be used to bond interfacial metallic substrates, then they are required to generate sufficient heat energy to melt SMs over a sufficiently long duration. Therefore, the Al NP/Al MP/Fe_2O_3 NP-based EM composites tested in the present study were finally selected as an optimized heating element for the interfacial bonding process.

To examine the effect of the amount of Fe_2O_3 NPs on the ignition and combustion properties of an Al NP/Al MP matrix, various Al NP/Al MP pellets with different amounts of Fe_2O_3 NP were fabricated and tested as shown in Fig. 4. There was no successful ignition in the case of the Fe_2O_3 NPs (10–20 wt%) in the Al MP/Al NP matrix, as shown in Fig. 4a. This was presumably because the amount of oxidizer was not sufficient to initiate the ignition and subsequent combustion of the fuel metals. However, when the amount of Fe_2O_3 NPs in the Al MP/Al NP matrix was $\geq$ 30 wt%, stable ignition and combustion could be achieved. Once the pellet was ignited, the flame propagated to the end of the pellet without stopping. Figure 4b shows the burn rate and total burning time of Al NP/Al MP composite pellets with different Fe_2O_3 NP contents (10–70 wt%), as measured using a high-speed camera. The burn rate increased steeply as the amount of Fe_2O_3 NPs was increased to around 40 wt%, and then increased gradually as the amount of Fe_2O_3 NPs was increased from 40–70 wt%. Simultaneously, the total burning time was the longest when the amount of Fe_2O_3 NPs was around 30 wt%, but then gradually decreased as the amount of Fe_2O_3 NPs was increased to $\geq$ 40 wt%. It is preferable for the burn rate of the Al NP/Al MP/Fe_2O_3 NP composite pellets to be such that the total burning time is longer, allowing the SMs (heated by the EMs) to melt sufficiently and eventually bond with the interfacial substrates. Therefore, the use of fuel-rich Al NP/Al MP (60–70 wt%) with an Fe_2O_3 NP content of 30–40 wt% is preferred for the interfacial bonding process, because the combustion properties are much less active than those in the stoichiometric condition (i.e., Al (25 wt%)/Fe_2O_3 (75 wt%)).

To determine the optimum heating pellet conditions for the interfacial bonding process, we examined the heat energy generated by Al NP/Al MP composites by varying the Fe_2O_3 NP content (20–70 wt%) using DSC, as shown in Fig. 5a. The first exothermic reaction was an aluminothermic reaction (i.e., $2Al + Fe_2O_3 \rightarrow Al_2O_3 + 2Fe + \Delta H$) in a temperature range of 500–600 °C. The second exothermic reaction usually occurred in a temperature range of 700–1000 °C due to the oxidation of the unreacted Al, which melted at around 670 °C. This was an endothermic reaction. This was clearly corroborated by DSC analyses for the Al NP/Fe_2O_3 NP and Al MP/Fe_2O_3 NP as shown in Fig. S2 in Supporting information. Figure 5b summarizes the evolution of the total heat energy of the exothermic reactions for various Al MP/Al NP/Fe_2O_3 NP (20–70 wt%) composites. The generated heat energy was found to increase with the amount of Fe_2O_3 NP ($\leq$ 40 wt%) in the Al MP/Al NP matrix, but it then decreased with the addition of further Fe_2O_3 NP ($>$ 40 wt%). This suggests that the optimized Fe_2O_3 NP content in the Al MP/Al NP matrix was around 40 wt%, which was found to maximize the aluminothermic and oxidation reactions of Al. However, the experimentally determined values for the total heat energy ($\leq$ 2.0 kJ g^{-1}) were much lower than the theoretical value of 3.9 kJ g^{-1}. We believe that this shortfall occurred due to (i) an oxide layer forming on the surfaces of the Al NPs and Al MPs and (ii) the incomplete oxidation of the Al MPs. This was corroborated by XRD analyses of the reactants and byproducts before and after the ignition test with the Al MP/Al NP/Fe_2O_3 composite powders, as shown in Fig. S3 in Supporting information. To achieve effective interfacial bonding, it is important to generate a sufficiently high amount of heat energy from a heating pellet for a sufficiently long duration. As a result of the present study, we found that the

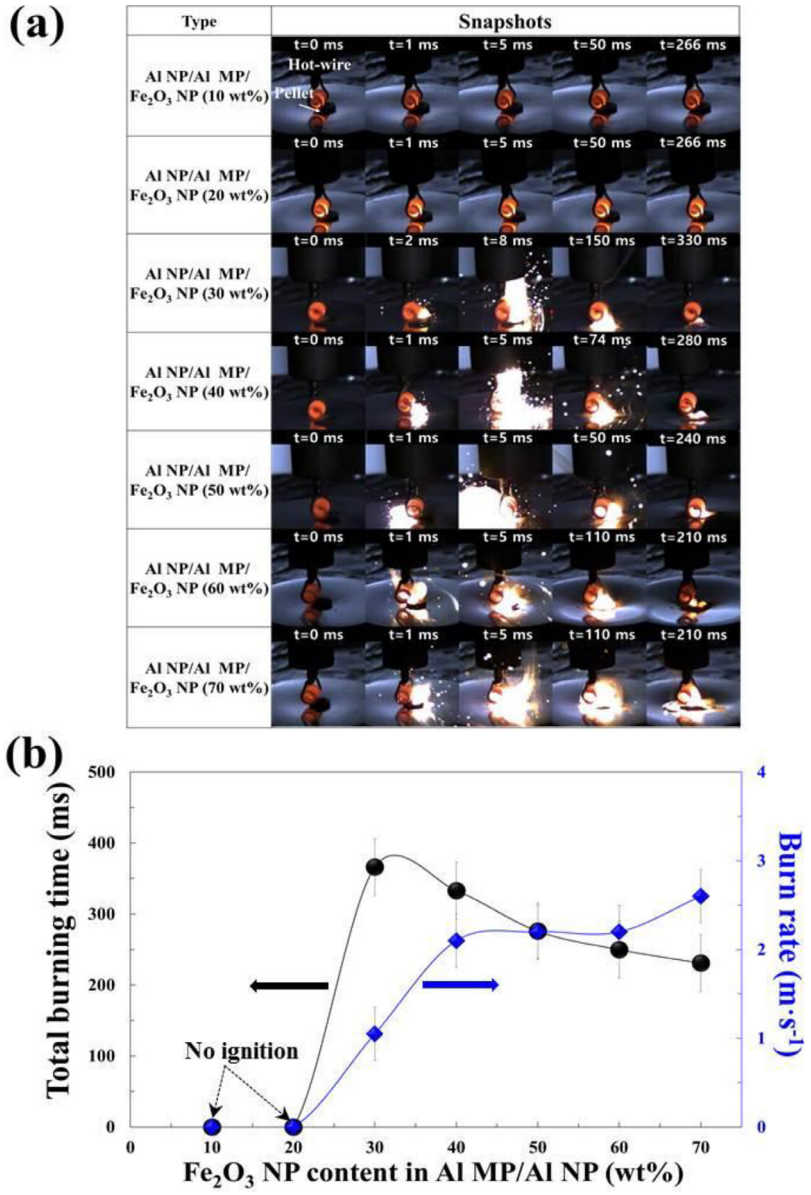

Fig. 4. (a) Images and (b) evolution of burn rate and total burning time of Al NP/Al MP composite pellets for different Fe_2O_3 NP contents.

optimum heating pellet consisted of an optimized Al NP/Al MP composite (60 wt%) to which we added Fe_2O_3 NP (around 40 wt%).

SEM analyses were performed to examine the structures of the SM/EM/SM multilayer pellets fabricated in the present study, as shown in Fig. 6. Top and side views of interfacial Cu substrates with SM/EM/SM multilayer pellets are shown in Fig. 6a. Figure 6c shows a cross-sectional SEM image of a SM/EM/SM pellet, fabricated using a die-compression molding process. The thicknesses of the SM and EM layers were found to be around 300 µm and 900 µm, respectively. Figure 6b shows that the primary particles of Al MP/Al NP/Fe_2O_3 NP in the EM layer strongly adhered to each other. Figure 6d shows the boundary layer between the SM and EM layers, which are tightly bonded by the compression process. As shown in Fig. S4 in Supporting information, the SAC305 powder accumulated in the SM layer, and was observed to consist of spherical particles having an average diameter of around 65 µm. However, they appeared to bond strongly while simultaneously undergoing plastic deformation by the pressurization process during pelletization.

To realize interfacial bonding, the SM/EM/SM multilayer pellets fabricated in this study were installed between Cu substrates measuring 15 mm × 23 mm, as shown in Fig. 7a and b. The SM/EM/SM multilayer pellet was composed of two parts: (i) The first half of the pellet was composed of an EM layer (i.e., Al MPs/Al NPs/Fe_2O_3 NPs) without an SM layer. This acted as an igniter. (ii) The second half of the pellet, composed of SM/EM/SM multilayers, was fabricated to bond to the interfacial Cu substrates (Fig. 7a). As a result of the ignition and combustion processes of the SM/EM/SM multilayer pellet, the interfacial Cu substrates were found to be successfully bonded by the application of a pressure of around 1 MPa, as shown in Fig. 7b and c. This suggests that the SM layer was sufficiently melted by the heat energy generated by the combustion of the EM layer, after which the interfacial Cu substrates were strongly bonded by the solder, once it solidified through its natural cooling process. Figure 7d shows a cross-sectional SEM image and the elemental mapping of the Cu substrates, interfacially bonded using the SM/EM/SM multilayer pellets. The Al MPs/Al NPs/Fe_2O_3 NPs in the EM layer and solder MPs in the SM layer were

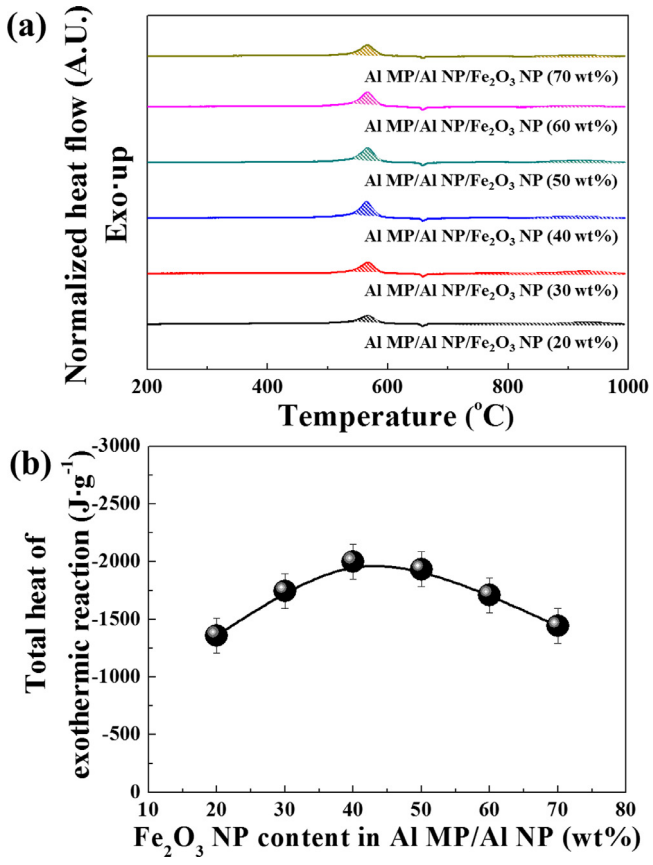

Fig. 5. (a) Differential scanning calorimetry (DSC) results and (b) total heat energy generated by exothermic and oxidation reactions of Al MP/Al NP composite by varying the amount of Fe_2O_3 NPs.

observed to be fully sintered and, simultaneously, the solder MPs were strongly attached to the surface of the Cu substrate. After the aluminothermic reaction of the EM layer, Fe and Al_2O_3 composites were formed; thus, Al, Fe, and O elements were observed in the EM layer. The SM and EM layers were strongly attached, but no atomic diffusion was observed. However, a very thin inter-metallic diffusion layer of Sn and Cu was formed between the Cu substrates and SM layers. In general, inter-metallic compounds of the Cu_6Sn_5 and Cu_3Sn phases are known to be formed by the reaction of Sn and Cu, diffused by heat generated in the interfacial bonding process. The thermal diffusion of Sn and Cu seemed to actively occur when relatively high temperatures were maintained for a relatively long duration. It is interesting to note that the thickness of the inter-metallic diffusion layer was less than 5 μm, but this increased considerably up to around 80 μm when the interfacial Cu substrates were bonded by the pure SM layer, which was heated in a furnace for a much longer duration, as shown in Fig. S5 in Supporting information.

After the interfacial bonding process, a universal tensile strength test was performed to examine the mechanical bonding strength between the Cu substrates, as shown in Fig. 8. For comparison, an SM layer pellet without the addition of an EM layer was first used to bond the interfacial Cu substrates. In this case, an enclosed furnace was used as an external heat energy source to preheat the Cu substrates to 300 °C for 30 min. After the preheating, the SM layer pellet was inserted between the Cu substrates, which were again heated to 300 °C for 1 h to attain interfacial bonding. A universal tensile strength test was performed, which revealed the maximum tensile stress and Young's modulus of the Cu substrates, interfacially bonded using the SM layer pellet, to be around 26.28 ± 0.26 MPa and 1741.12 ± 17.41, respectively. However, when we applied the SM/EM/SM multilayer pellet to the interfacial bonding process, the resulting maximum tensile strength and Young's modulus were found to be around 36.48 ± 0.36 MPa

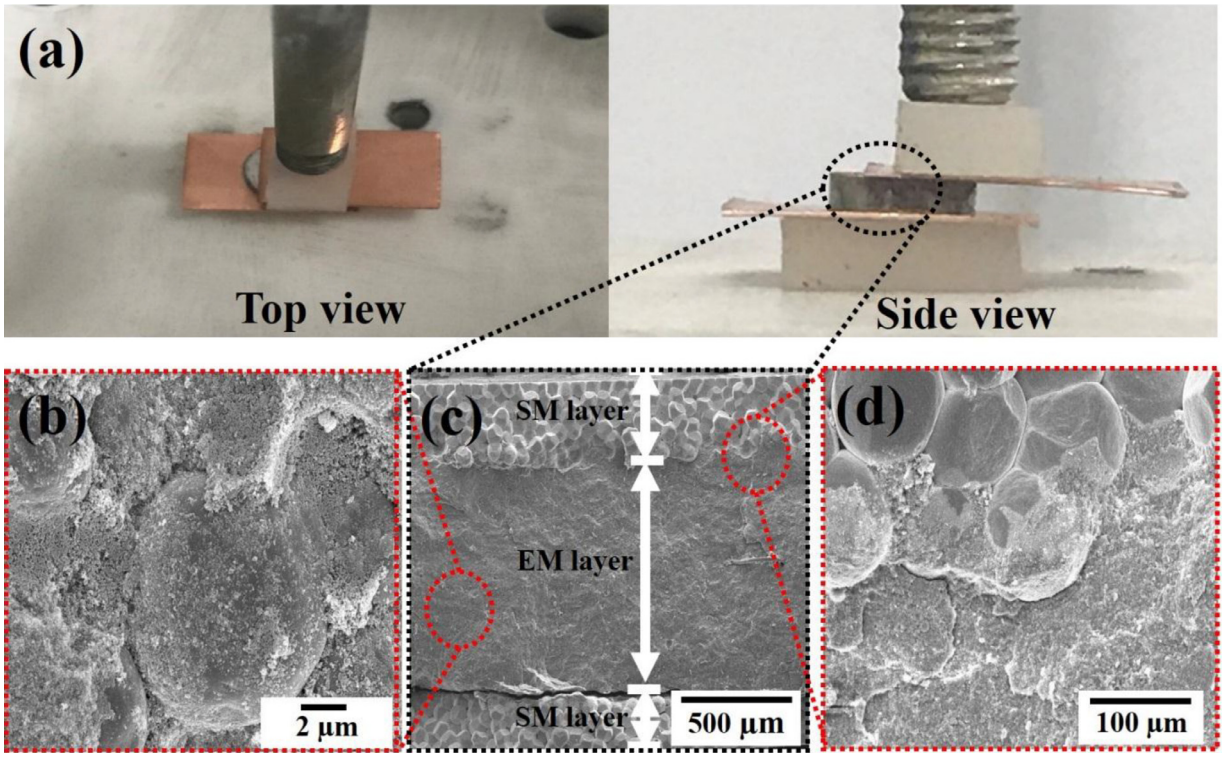

Fig. 6. (a) Top- and side-views of SM/EM/SM multilayer pellet inserted between interfacial Cu substrates. Cross-sectional SEM images of (b) EM layer, (c) SM/EM/SM multilayer, and (d) interface between SM and EM layers.

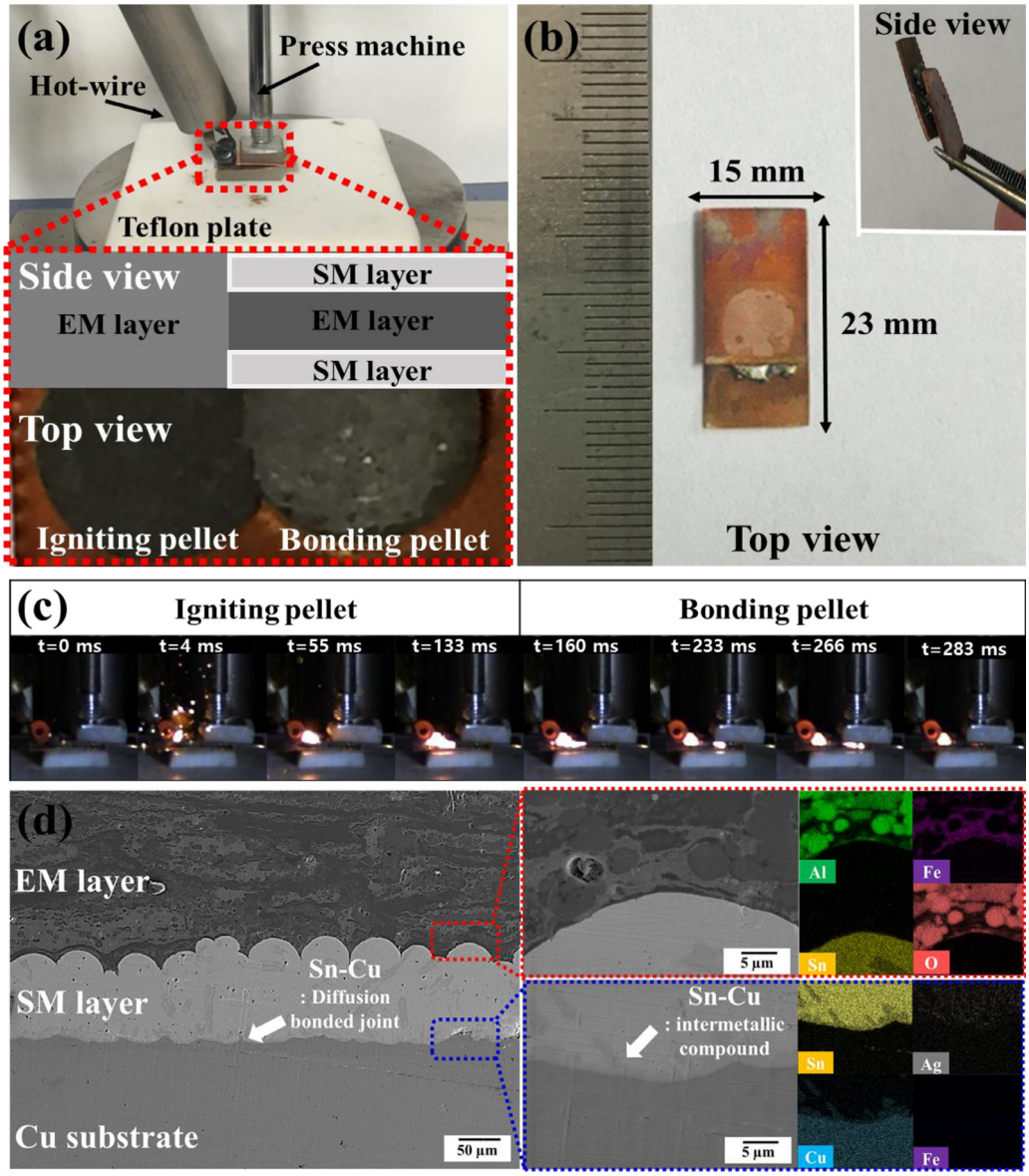

Fig. 7. (a) Cu substrates, composite pellet, and interfacial bonding devices and (b) interfacially bonded Cu substrates using SM/EM/SM multilayer pellet, (c) images of flame propagation through the first-half igniting pellet and second-half heating & bonding pellet, and (d) cross-sectional SEM images and elemental mappings of interfacial Cu substrates, physically bonded by SM/EM/SM composite pellet.

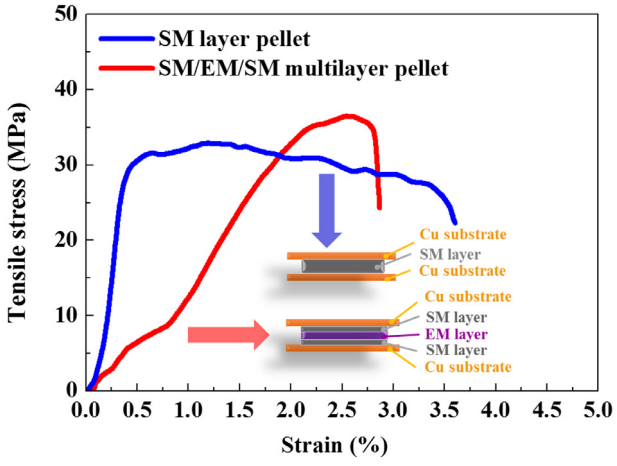

Fig. 8. Comparison of universal tensile strength test results for Cu substrates interfacially bonded using SM layer and SM/EM/SM multilayer pellets.

and 2469.26 ± 24.69, respectively, which were approximately 40% greater than those obtained with the SM layer pellet (without the EM layer). The strength and ductility of the Cu substrates bonded using the SM/EM/SM multilayer pellet were much better than those that were interfacially bonded using the SM layer pellet. Highly brittle property was observed for interfacial bonding made by SM layer-based pellet because relatively thick intermetallic compound was formed by relatively long heating process in the furnace (see Fig. S5). This suggests that the SM/EM/SM multilayer pellets fabricated in the present study can attain an excellent mechanical bonding strength between the interfacial metallic substrates with the advantages of simple, easy, and versatile welding and bonding applications.

4. Conclusions

In the present study, we examined the effects of micro- and nanoscale EMs as a heat energy source for melting SMs in the interfacial bonding process for metallic substrates. The EM layers

were composed of Al MPs (fuel), Al NPs (fuel), and Fe_2O_3 NPs (oxidizer), respectively. The Al NPs (30 wt%)/Al MPs (30 wt%)/Fe_2O_3 NP (40 wt%) composite powders were found to have the highest exothermic energy and a sufficiently long combustion duration. The presence of Al NPs was essential to the stable ignition and initiation of Al MPs, which were also required to attain longer combustion duration. This suggests that the use of highly reactive Al NPs/Fe_2O_3 NPs in EM composites can improve the aluminothermic reaction, while the addition of Al MPs to the Al NPs/ Fe_2O_3 NPs is also required to maintain their high thermal energy for a longer duration. Finally, the interfacial bonding process between Cu substrates was successfully demonstrated using SM/EM/SM multilayer pellets. The resulting mechanical bonding strength for interfacially bonded Cu substrates using SM/EM/SM multilayer pellets was found to be around 40% better than that attainable with SM layer pellets. This suggests that the micro- and nanoscale EMs were effective heat energy sources for melting SMs so that the interfacial bonding process suggested in this study can realize simple, easy, and versatile welding and bonding applications.

Author contributions

Both K. J. Kim and M. H. Cho equally contributed to this work as first authors.

Conflict of interest

The authors declare no competing financial interest.

Supporting information

Brief statement in nonsentence format listing the contents of the material supplied as Supporting information.

Acknowledgments

This research was supported by the Civil & Military Technology Cooperation Program through the National Research Foundation of Korea (NRF) funded by the Ministry of Science, ICT & Future Planning (No. 2013M3C1A9055407). This research was also supported by the Basic Science Research Program through the National Research Foundation of Korea (NRF) funded by the Ministry of Education and the Ministry of Science, ICT & Future Planning (No. 2015R1A2A1A15054036 & 2016R1A6A3A11935550).

Supplementary materials

Supplementary material associated with this article can be found, in the online version, at doi:10.1016/j.combustflame.2018.08.016.

References

[1] M. Chen, L. Yuan, S Liu, Research on low-temperature anodic bonding using induction heating, Sens. Actuator A – Phys. 133 (1) (2007) 266–269.
[2] Y.H. Ko, J.D. Lee, T. Yoon, C.W. Lee, T.S Kim, Controlling interfacial reactions and intermetallic compound growth at the interface of a lead-free solder joint with layer-by-layer transferred graphene, ACS Appl. Mater. Interface 8 (8) (2016) 5679–5686.
[3] J.H. Kweon, J.W. Jung, T.H. Kim, J.H. Choi, D.H Kim, Failure of carbon composite-to-aluminum joints with combined mechanical fastening and adhesive bonding, Compos. Struct. 75 (1) (2006) 192–198.
[4] M. Yang, H. Ji, S. Wang, Y.H. Ko, C.W. Lee, J. Wu, M Li, Effects of Ag content on the interfacial reactions between liquid Sn–Ag–Cu solders and Cu substrates during soldering, J. Alloy Compd. 679 (2016) 18–25.
[5] T.H. Kim, M.M.R. Howlader, T. Itoh, T Suga, Room temperature Cu–Cu direct bonding using surface activated bonding method, J. Vac. Sci. Technol. A 21 (2) (2003) 449–453.
[6] Y. Kobayashi, T. Shirochi, Y. Yasuda, T Morita, Metal–metal bonding process using metallic copper nanoparticles prepared in aqueous solution, Int. J. Adhes. Adhes. 33 (2012) 50–55.
[7] P. Peng, A. Hu, A.P. Gerlich, G. Zou, L. Liu, Y.N. Zhou, Joining of silver nanomaterials at low temperatures: processes, properties, and applications, ACS Appl. Mater. Interface 7 (23) (2015) 12597–12618.
[8] Z.J. Jia, Q. Fang, Z.L Fang, Bonding of glass microfluidic chips at room temperatures, Anal. Chem. 76 (18) (2004) 5597–5602.
[9] V.G. Kutchoukov, F. Laugere, W. van Der Vlist, L. Pakula, Y. Garini, A Bossche, Fabrication of nanofluidic devices using glass-to-glass anodic bonding, Sens. Actuators A – Phys. 114 (2) (2004) 521–527.
[10] Y. Sun, Y.C. Kwok, N.T Nguyen, Low-pressure, high-temperature thermal bonding of polymeric microfluidic devices and their applications for electrophoretic separation, J. Micromech. Microeng. 16 (8) (2006) 1681–1688.
[11] P.J. Mutton, E.F Alvarez, Failure modes in aluminothermic rail welds under high axle load conditions, Eng. Fail. Anal. 11 (2) (2004) 151–166.
[12] C. Merıc, E. Atık, S Şahın, Mechanical and metallurgical properties of welding zone in rail welded via thermite process, Sci. Technol. Weld. Join. 7 (3) (2002) 172–176.
[13] K. Aran, L.A. Sasso, N. Kamdar, J.D Zahn, Irreversible, direct bonding of nanoporous polymer membranes to PDMS or glass microdevices, Lab Chip 10 (5) (2010) 548–552.
[14] C.W. Tsao, D.L DeVoe, Bonding of thermoplastic polymer microfluidics, Microfluid Nanofluid 6 (1) (2009) 1–16.
[15] C. Lee, W.F. Huang, J.S Shie, Wafer bonding by low-temperature soldering, Sens. Actuator A – Phys. 85 (1) (2000) 330–334.
[16] S. Kikuchi, M. Nishimura, K. Suetsugu, T. Ikari, K Matsushige, Strength of bonding interface in lead-free Sn alloy solders, Mat. Sci. Eng. A – Struct. 319 (2001) 475–479.
[17] R.I. Made, C.L. Gan, L.L. Yan, A. Yu, S.W. Yoon, J.H. Lau, C Lee, Study of low-temperature thermocompression bonding in Ag-In solder for packaging applications, J. Electron. Mater. 38 (2) (2009) 365.
[18] M.O. Alam, Y.C. Chan, K.N. Tu, Effect of 0.5 wt% Cu in Sn– 3.5% Ag solder on the interfacial reaction with Au/Ni metallization, Chem. Mater. 15 (23) (2003) 4340–4342.
[19] S. Nambu, M. Michiuchi, J. Inoue, T Koseki, Effect of interfacial bonding strength on tensile ductility of multilayered steel composites, Compos. Sci. Technol. 69 (11) (2009) 1936–1941.
[20] H. Nakanishi, T. Nishimoto, R. Nakamura, A. Yotsumoto, T. Yoshida, S Shoji, Studies on SiO_2–SiO_2 bonding with hydrofluoric acid. Room temperature and low stress bonding technique for MEMS, Sens. Actuators A – Phys. 79 (3) (2000) 237–244.
[21] J. Wang, E. Besnoin, O.M. Knio, T.P Weihs, Investigating the effect of applied pressure on reactive multilayer foil joining, Acta Mater. 52 (18) (2004) 5265–5274.
[22] Y.T. Cheng, W.T. Hsu, K. Najafi, C.C. Nguyen, L Lin, Vacuum packaging technology using localized aluminum/silicon-to-glass bonding, J. Microelectromech. Syst. 11 (5) (2002) 556–565.
[23] R. Tadepalli, C.V Thompson, Formation of Cu–Cu interfaces with ideal adhesive strengths via room temperature pressure bonding in ultrahigh vacuum, Appl. Phys. Lett. 90 (15) (2007) 151919.
[24] M.O. Alam, Y.C. Chan, K.N. Tu, J.K. Kivilahti, Effect of 0.5 wt% Cu in Sn– 3.5% Ag solder balls on the solid state interfacial reaction with Au/Ni/Cu bond pads for Ball Grid Array (BGA) applications, Chem. Mater. 17 (9) (2005) 2223–2226.
[25] C.E. Ho, Lin Y. L., C.R. Kao, Strong effect of Cu concentration on the reaction between lead-free microelectronic solders and Ni, Chem. Mater. 14 (3) (2002) 949–951.
[26] M. Burda, A. Lekawa-Raus, A. Gruszczyk, K.K Koziol, Soldering of carbon materials using transition metal rich alloys, ACS Nano 9 (8) (2015) 8099–8107.
[27] F. Kim, J. Luo, R. Cruz-Silva, L.J. Cote, K. Sohn, J Huang, Self-propagating domino-like reactions in oxidized graphite, Adv. Funct. Mater. 20 (17) (2010) 2867–2873.
[28] J.H. Kim, J.Y. Ahn, H.S. Park, S.H. Kim, Optical ignition of nanoenergetic materials: the role of single-walled carbon nanotubes as potential optical igniters, Combust. Flame 160 (4) (2013) 830–834.
[29] S.H. Kim, M.R Zachariah, Enhancing the rate of energy release from nanoenergetic materials by electrostatically enhanced assembly, Adv. Mater. 16 (20) (2004) 1821–1825.
[30] W.P. King, S. Saxena, B.A. Nelson, B.L. Weeks, R Pitchimani, Nanoscale thermal analysis of an energetic material, Nano Lett. 6 (9) (2006) 2145–2149.
[31] G. Jian, J. Feng, R.J. Jacob, G.C. Egan, M.R. Zachariah, Super-reactive Nanoenergetic Gas Generators Based on Periodate Salts, Angew. Chem. Int. Ed. 52 (37) (2013) 9743–9746.
[32] M.M. Biss, Energetic material detonation characterization: a laboratory-scale approach, Propellants Explos. Pyrotech. 38 (4) (2013) 477–485.
[33] N.S. Jang, S.H. Ha, K.H. Kim, M.H. Cho, S.H. Kim, J.M Kim, Low-power focused-laser-assisted remote ignition of nanoenergetic materials and application to a disposable membrane actuator, Combust Flame 182 (2017) 58–63.
[34] L. Marín, C.E. Nanayakkara, J.F. Veyan, B. Warot-Fonrose, S. Joulie, A. Estève, C Rossi, Enhancing the reactivity of Al/CuO nanolaminates by Cu incorporation at the interfaces, ACS Appl. Mater. Interface 7 (22) (2015) 11713–11718.
[35] J. Kwon, J.M. Ducéfe´, P. Alphonse, M. Bahrami, M. Petrantoni, J.F. Veyan, Y.J Chabal, Interfacial chemistry in Al/CuO reactive nanomaterial and its role in exothermic reaction, ACS Appl. Mater. Interface 5 (3) (2013) 605–613.
[36] F. Séverac, P. Alphonse, A. Estève, A. Bancaud, C. Rossi, High-energy Al/CuO nanocomposites obtained by DNA-directed assembly, Adv. Funct. Mater. 22 (2) (2010) 323–329.

[37] M.L. Pantoya, J.J. Granier, Combustion behavior of highly energetic thermites: nano versus micron composites, Propellants Explos. Pyrotech. 30 (1) (2005) 53–62.
[38] J. Lin, M. Guo, C.T. Yip, W. Lu, G. Zhang, X. Liu, L. Zhou, X. Chen, H Huang, High temperature crystallization of free-standing anatase TiO_2 nanotube membranes for high efficiency dye-sensitized solar cells, Adv. Funct. Mater. 23 (10) (2013) 5952–5960.
[39] K. Zhang, C. Rossi, M. Petrantoni, N Mauran, A nano initiator realized by integrating Al/CuO-based nanoenergetic materials with a Au/Pt/Cr microheater, J. Microelectromech. Syst. 17 (4) (2008) 832–836.
[40] J.L. Cheng, H.H. Hng, Y.W. Lee, S.W. Du, N.N. Thadhani, Kinetic study of thermal- and impact-initiated reactions in Al-Fe_2O_3 nanothermite, Combust. Flame. 157 (2010) 2241–2249.
[41] Y. Wang, X. Song, W. Jiang, G Deng, X. Guo, H. Liu, F. Li, Mechanism for thermite reactions of aluminum/iron-oxide nanocomposites based on residue analysis, Trans. Nonferrous Met. Soc. China 24 (2014) 263–270.